Article

Not peer-reviewed version

A Novel Noninvasive Murine Model of Neonatal Hypoxic Ischemic Encephalopathy Demonstrates Developmental Delay and Motor Deficits with Activation of Inflammatory Pathways in Monocytes

Elise A. Lemanski , Bailey A. Collins , Andrew T. Ebenezer , Sudha Anilkumar , Victoria Langdon , Qi Zheng , Shanshan Ding , Karl Franke , Jaclyn M. Schwarz , Elizabeth Wright-Jin *

Posted Date: 30 July 2024

doi: 10.20944/preprints202407.2364.v1

Keywords: hypoxic ischemic encephalopathy; maternal immune activation; motor; development; microglia; macrophages

Article

A Novel Noninvasive Murine Model of Neonatal Hypoxic Ischemic Encephalopathy Demonstrates Developmental Delay and Motor Deficits with Activation of Inflammatory Pathways in Monocytes

Elise A. Lemanski [1,2], Bailey Collins [1,2], Andrew T. Ebenezer [1], Sudha Anilkumar [1,2], Victoria Langdon [1], Qi Zheng [1], Shanshan Ding [3], Karl Franke [1], Jaclyn Schwarz [2] and Elizabeth Wright-Jin [1,2,4,5,*]

[1] Nemours Children's Health, Division of Biomedical Research
[2] University of Delaware, Psychological and Brain Sciences
[3] University of Delaware, Applied Economics and Statistics, Center for Bioinformatics and Computational Biology
[4] Nemours Children's Health, Division of Neurology
[5] Thomas Jefferson University, Sidney Kimmel Medical College
* Correspondence: author: Elizabeth Wright-Jin, MD, PhD, Nemours Children's Health, 1600 Rockland Rd, Wilmington, DE 19803, Elizabeth.wright-jin@nemours.org

Abstract: Neonatal hypoxic ischemic encephalopathy (HIE) occurs in 1.5 per 1000 live births, leaving affected children with long-term motor and cognitive deficits. Few animal models of HIE incorporate maternal immune activation (MIA) despite the significant risk MIA poses to HIE incidence and diagnosis. Our non-invasive model of HIE pairs late gestation MIA with postnatal hypoxia. HIE pups exhibited a trend toward smaller overall brain size and delays in the ontogeny of several developmental milestones. In adulthood, HIE animals had reduced strength and gait deficits, but no difference in speed. Surprisingly, HIE animals performed better on the rotarod, an assessment of motor coordination. There was significant upregulation of inflammatory genes in microglia 24 hours after hypoxia. Single cell RNAseq revealed two microglia subclusters of interest following HIE. Pseudobulk analysis revealed increased microglia motility gene expression and upregulation of epigenetic machinery and neurodevelopmental genes in macrophages following HIE. No sex differences were found in any measures. These results support a two-hit noninvasive model pairing MIA and hypoxia as a model for HIE in humans. This model results in a milder phenotype compared to established HIE models; however, HIE is a clinically heterogeneous injury resulting in a variety of outcomes in humans. The pathways identified in our model of HIE may reveal novel targets for therapy for neonates with HIE.

Keywords: Hypoxic ischemic encephalopathy; maternal immune activation; motor; development; microglia; macrophages

1. Introduction

Neonatal hypoxic ischemic encephalopathy (HIE) is a common brain injury that affects infants born at term with an estimated incidence of 1-3 per 1000 births in developed countries and 26-30.6 per 1000 births in underdeveloped countries **[1,2]**. HIE can be caused by a myriad of birth complications including placental abruption, uterine rupture, cord prolapse, chorioamnionitis, and maternal hypotension. Ultimately, these factors lead to insufficient delivery of oxygen to the fetal brain, resulting in the risk of permanent brain injury. Children with severe HIE have a mortality rate of up to 50% and those who survive can have significant long-term neurologic deficits including cerebral palsy, epilepsy, and vision/hearing impairments **[3,4]**. Therapeutic hypothermia is the only effective therapy for HIE and involves cooling the infant to a temperature of 33.5°C for 72 hours **[5]**. Despite the success of this therapy in improving outcomes, up to 40% of neonates who receive this

 doi:10.20944/preprints202407.2364.v1

treatment still suffer brain injury and disability **[5,6]**. To be effective, therapeutic hypothermia must be initiated in the first 6 hours of life. If clinical signs of hypoxia are missed, the infant can quickly move out of this narrow window for treatment **[7]**. This demonstrates the critical need for additional neurotherapeutics to mitigate brain injury and reduce lifelong disabilities following neonatal HIE.

One of the most prominent risk factors for HIE is inflammation. Forty to fifty percent of neonates affected by neonatal HIE are born to mothers with chorioamnionitis or clinical signs of this infection, such as fever and leukocytosis **[8]**. However, most preclinical models of HIE do not take inflammation into account [9]. Maternal immune activation (MIA) is a well-established model of inflammation that uses a peripheral injection of lipopolysaccharide (LPS) during gestation to elicit an immune response **[10]**. LPS is a bacterial cell wall-derived endotoxin that binds to toll-like receptor 4 (TLR4) on immune cells to stimulate the production of immune molecules, including cytokines, in the dam **[11]**. This immune response is also triggered in the fetus by the transmission and production of cytokines through the placenta **[10,12]**. Although maternal infection is a known risk factor for developmental delays and disorders in humans, most cases of maternal infection or inflammation do not lead to these outcomes **[13]**. Therefore, it is hypothesized that maternal immune activation may have a priming effect that leads to increased susceptibility to environmental or genetic "second hits'', further increasing the risk of developing various CNS disorders **[14,15]** depending on the timing, severity, and type of cumulative stressors **[16]**.

Our novel model of neonatal HIE, characterized here, combines MIA via systemic LPS injection in late gestation with a short but severe global hypoxia at postnatal day 6 (P6). Exposure to LPS during late pregnancy effectively simulates chorioamnionitis and is used in other models of this common pregnancy complication **[17]**. Utilizing MIA prior to hypoxia allows for the investigation of the interaction of etiologically relevant maternal, placental, and neonatal inflammatory factors that contribute to the complex brain injury of HIE around the time of birth. We excluded the carotid artery ligation used in the popular Rice-Vannucci model due to the substantial hemispheric ischemic damage that this model evokes. We sought to thoroughly characterize our model of HIE to investigate whether it recapitulates the outcomes and symptomatology present in humans. This characterization includes investigating the changes within microglia following injury, gross changes in brain volume 24 hours following the second hit of hypoxia, determining whether this model leads to developmental delays in the neonatal period, and determining long-term deficits in motor and social function. These results help validate the proposed model and inform metrics to examine treatments tested within this model.

2. Materials and Methods

2.1. Mouse Strains

CF-1 mice were acquired from Charles River as timed pregnant dams. Mice had a 12-hour light-dark cycle with free access to food and water. Determination of sex in neonatal mice less than 10 days old was achieved by genotyping for *Sry* using the following primers.

SRY F: TTG TCT AGA GAG CAT GGA GGG CCA TGT CAA
SRY R: CCA CTC CTC TGT GAC ACT TTA GCC CTC CGA

2.2. Maternal Immune Activation

Timed pregnant mice were injected with 50 micrograms/kg body weight lipopolysaccharide (LPS) or 0.05 ml 0.9% sterile saline via intraperitoneal injection on gestational day 18 (E18). Dosing of LPS was determined via survival analysis of dams and litters with poor survival at higher doses.

2.3. Hypoxia Exposure

Adapted from Aravamuthan et al., 2020, *Neurobiology of Disease* **[18]**. Postnatal day 6 (P6) was chosen for hypoxia administration due to poor animal survival at later time points. Mice were placed in a hypoxia chamber (Biospheryx) on a heated pad (37.2 °C) and subjected to 8 minutes of either progressive hypoxia from 21% to 0% oxygen or normoxia (21% oxygen) (**Figure 1**). After 8 minutes

 doi:10.20944/preprints202407.2364.v1

of hypoxia, the chamber door was opened to allow rapid recovery to 21% oxygen. Surviving mice were returned to their mother for further recovery.

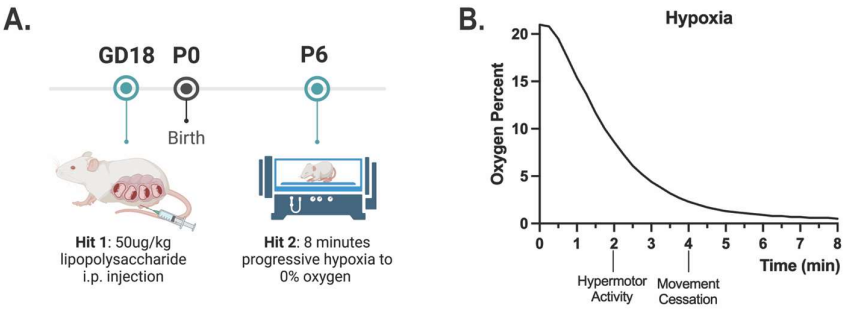

Figure 1. Two-hit HIE model. (A) A representation of our two-hit model of HIE. (B) Representative graph of oxygen levels present and pup behavior during the 8-minute hypoxia protocol (N = 3 litters).

2.4. Neonatal Development Testing

On the day of birth (P0), the number of offspring was counted, and the pups weighed. Litters were culled to a maximum of ten pups, and litters of less than six pups were excluded, to control for differences in behavior that could be attributed to litter size induced by the abortifacient effects of LPS (Supplemental Figure 1A). Beginning on P1, between two and four males and females from each litter were examined daily for the acquisition of typical developmental milestones and reflexes. Testing was performed at the same time each day. The pups from each litter were removed from the dam and kept on a heating pad at 37°C to maintain a stable body temperature during testing. The means from the males and females from each litter were used for statistical comparisons to avoid litter effects. Testing for each reflex began three days prior to the typical onset of the behavior, when possible, and was performed until the response was observed for two consecutive days. Behavioral tests were adapted from Hill et al., 2008, *Neuropeptide Techniques*, including eye opening, surface righting, negative geotaxis, rooting, forelimb grasp, auditory startle, open area traversal, and air righting [19]. Hindlimb splay, an assessment of gross motor function and muscle tone, was additionally included. For this test, beginning on P5, each pup was suspended from their tail, and hind limb extension was observed. When the pup fully extended both hindlimbs to 45 degrees, this was recorded as acquisition of hindlimb splay.

2.5. Adult Behavior

The following behavioral assessments were performed on adult mice beginning at P60.

Grip Strength. Mice were lowered to grab a triangular pull bar with their forelimbs on a grip strength meter (Columbus Instruments) and were pulled backwards by the tail until they lost their grip. Force in newtons applied to the bar before release was recorded across two trials and averaged.

Catwalk. Each mouse was placed on the platform on the CatWalk (Noldus) and the gait pattern of each mouse was captured videometrically and subsequently analyzed using the software package for the apparatus, Catwalk XT (Noldus). Three compliant trials with criteria of a minimum run duration of 0.5 seconds and a maximum run duration of 5 seconds were recorded per animal. Trials were additionally excluded if they did not meet the criteria of a minimum number of 10 consecutive steps per run, an average speed range from 30-90 cm/second, and a maximum speed variation of 40%, or if the animal stopped during the trial.

Rotarod. Mice were habituated to the apparatus in two 2-minute sessions 2-3 hours apart the day prior to testing at a constant speed of 4 rpm. On the day of testing each mouse was placed onto a moving drum of a Rotarod Treadmill for Mice (Ugo Basile). The rotarod treadmill was set to accelerate progressively from 4-40 rpm over 300 seconds. The amount of time the mouse remained moving on the drum was recorded. Three trials were performed with a 15-minute inter-trial interval.

 doi:10.20944/preprints202407.2364.v1

Sociability. Mice were placed in a plexiglass box 48" in length and 16" in height separated into three smaller chambers. On day 1 the mouse was habituated to the apparatus. The mouse was placed in the middle chamber and left to explore the apparatus for 5 minutes. The mouse was then removed, and an object was added to the cage in a lateral chamber, and a species-, sex- and age-matched novel mouse was added to the cage in the opposite chamber. The experimental mouse was then placed into the middle chamber and allowed to explore for 5 minutes. Sessions were video recorded, and the amount of time spent with the novel animal or the novel object were measured. Day 2 consisted of a social memory test. One chamber contained the familiar mouse from Day 1 and the other a new novel mouse. The experimental mouse was then placed into the center chamber and allowed to explore the apparatus for 5 minutes. Sessions were video recorded, and time spent with the novel or the familiar mouse was measured.

2.6. Structural MRI

Brains from a subset of offspring were collected on P7 for ex vivo MRI, 24 hours after hypoxia. A second cohort of both male and female offspring were collected at 24 hours following the completion of the adult behaviors (P74). Whole brains from both cohorts were collected for ex vivo MRI. MRI was performed with a Bruker Biospec 94/20 with a 9.4 Tesla magnet at the University of Delaware Center for Biomedical and Brain Imaging (CBBI). A T2 weighted 2D structural MRI was conducted on brains collected at P7. Manual segmentation was performed on structural scans to determine the relative size of the hippocampus, dorsal striatum, and cortex. In adult brains, a T2 weighted 3D structural scan was conducted to identify if structural differences persist into adulthood. Structural MRI scans were manually segmented for regions of interest (ROIs).

2.7. Bulk RNA-Sequencing

Sequencing. Whole brains were collected from male and female pups one day following the second hit of hypoxia (P7) and dissociated into a single cell solution using the Adult Brain Dissociation Kit and gentleMACS Octo Dissociator (Miltenyi Biotec). Microglia were enriched via magnetic CD11b-coated bead isolation (Miltenyi Biotec). RNA was extracted and prepared by the Pediatric Genomics Laboratory at Nemours Children's Health using the Illumina Stranded Total RNA Prep with Ribo Zero Plus. RNA sequencing was performed via Illumina NextSeq 500/550 High Output Kit v2.5 (300 cycles) conducted by the Pediatric Genomics Laboratory at Nemours Children's Health.

Bioinformatic Analysis. Bulk RNAseq libraries were mapped to the GRCm39 genome assembly using Sentieon's [20] accelerated version of the STAR [21] v2.7.10b algorithm. Gene counting was performed via RSEM [22] v1.3.1. Differential gene expression analysis was performed using edgeR [23] and DESeq2 [24] by taking a union of the results. Single cell mRNAseq libraries were mapped to the mm10 reference genome provided by 10x using Cellranger [25] v7.1 and downstream tertiary analysis was performed using Seurat v5 [26].

Gene set enrichment analysis. GSEA was performed using the GSEA and MSigDB software available as a joint project of UC San Diego and the Broad Institute [27]. GSEA Preranked analysis was performed using mouse hallmark gene sets [28] and the preranked expression from DEG log2FC results with an FDR adjusted p-value < .05. Cutoffs of nominal *p*-value of < .001 and FDR < .05 were used for inclusion of statistically relevant gene sets.

2.8. Single Cell RNA Sequencing

Whole brains were collected from male and female pups two days (P8) and four days (P10) day following the second hit of hypoxia. Single cell RNA sequencing (scRNAseq) was performed by creation of a single cell solution using the GentleMACS brain dissociator (Miltenyi Biotec) and Adult Brain Dissociation Kit (Miltenyi Biotec). Cell viability was confirmed via trypan blue staining. Live and dead cells were counted using a hemocytometer at 10x magnification. The 10x Genomics Chromium Next GEM Single Cell 3' Kit v3.1, Dual Index Kit TT Set A, Chromium Next GEM Chip G

 doi:10.20944/preprints202407.2364.v1

Single Cell Kit, and SPRIselect Reagent Kit were used for library creation. Sample and library quality control was achieved using Agilent High Sensitivity D5000 ScreenTape, D5000 Reagents, D5000 Ladder and KAPA Universal Library Quantification Kit. Sequencing was achieved using Illumina NextSeq 2000 P3 Reagents (100 cycles). All scRNAseq libraries were sequenced on an Illumina NextSeq 2000 instrument at the Nemours Research Lab with a 2 × 150 paired-end (PE) read setting. Raw FASTQ read files were called using the Illumina Dragen software (v4.2.7).

All scRNAseq libraries were sequenced on an Illumina NextSeq 2000 instrument at the Nemours Research Lab with a 2 × 150 paired-end (PE) read setting. Raw FASTQ read files were called using the Illumina NextSeq 1000/2000 Control Software (v1.5.0).

2.9. scRNAseq Data Processing and Statistical Analysis

The scRNAseq dataset was processed using the 10Xgenomics Cell Ranger "count" pipeline (v7.1.0) designed for the 3′ Gene Expression analysis. In essence, this pipeline first generates barcode-embedded FASTQ files ("mkfastq"), then calculates single-cell level feature/barcode count matrix ("count") for each sample, for which the Cell Ranger pre-built mm10-2020-A database (GENCODE vM23/Ensembl98) was used. All the scRNAseq count data were imported into an RStudio server at Nemours as R objects using the Seurat package (v5.1.0) [29,30], and subsequent statistical and visualization analyses were performed on the RStudio server using R packages such as Seurat, DESeq2, and gprofiler2 [24,29–31]. To be specific, Seurat objects for all samples were merged into a single integrated object using the Seurat v5 integration procedure, and cell clusters were identified using the shared nearest neighbor (SNN) method based on the integrated data. To annotate the cell clusters, we downloaded known gene markers of potential cell types from brain tissues from the PanglaoDB and CellMarker 2.0 databases [32,33] (Supplementary File S1), then cross-examined the expression profiles of the marker genes in the cell clusters, so we can manually annotate Seurat identified cell clusters. Notably, a few cell clusters failed being annotated using the known markers. For this unknown cluster, we identified conserved markers using the "FindConservedMarkers" function from Seurat and manually annotated them as the endothelial cells based on prior knowledge of function associated with these gene markers. To identify subclusters for given cell types including microglia, macrophages, and T/B-cells, we subset the original integrated dataset based on the cell type annotations, then performed sub-cluster analysis for each aforementioned cell type similarly as for the overall dataset. To identify differentially expressed genes (DE-genes) between different treatment conditions, we generated "pseudobulk" RNAseq objects from Seurat where single-cell expression profiles from the same sample were aggregated, and further converted them into pseudobulk RNAseq datasets using the DESeq2 package. DE-genes of various comparisons were identified by negative binomial models using the DESeq2 package [24]. Finally, the functional and pathway enrichment analysis was performed using the gost function from the gprofiler2 package [31].

2.10. Statistics

Behavior. Statistical analyses were performed using GraphPad Prism (version 10.2.0). Comparisons were initially made with two-way ANOVA using sex and HIE treatment as factors. When there was no main effect or interaction with sex, males and females were collapsed and an unpaired t-test was conducted. All data was tested for normality prior to further analysis. In the cases where data was not normally distributed, non-parametric tests were used. For the acquisition of neonatal behaviors, males and females were averaged for each litter for a total of two data points per litter, as litter effects are particularly prominent in the neonatal period [19]. The data from individual animals were analyzed for adult behavior to capture the full variance of adult behavior. Data are shown as mean +/- SEM, with individual data points included on graphs. $p < 0.05$ was considered statistically significant.

Rotarod. Statistical analysis was conducted on R (version 4.3.3). Data was not normally distributed due to a cutoff of 300 seconds. To take both latency and censorship into account across trials a cox mixed effects model "*coxme()*" was used. The model incorporated fixed effects of treatment

 doi:10.20944/preprints202407.2364.v1

and sex, random effects of trial and trial/treatment, and a nested factor of 1. Sex was collapsed when no significant main effect or interaction with sex was found. A p value less than 0.05 was considered statistically significant.

3. Results

3.1. Non-Invasive Two Hit Model of Neonatal HIE Produces Developmental Delays and Reduction in Brain Volume

Our non-invasive model utilizes a first hit of systemic maternal immune activation via a 50 μg/kg dose of lipopolysaccharide (LPS) on gestational day 18 (**Figure 1A**). Controls were administered 0.05 mL saline. In mice, gestation typically lasts an average of 20 days, and GD18 is equivalent to the third trimester in humans **[34]**. On postnatal day 6, pups were exposed to 8 minutes of progressive hypoxia from ambient oxygen levels of 21% oxygen to 0% oxygen (**Figure 1B**). Controls were placed in the same hypoxia chamber but were maintained at ambient oxygen levels for the entire 8 minutes. On P7, 24 hours following hypoxia, brains were collected for ex vivo anatomical MRI to assess for differences in overall brain volume as well as relative brain region volume. Animals exposed to maternal immune activation alone were included in this assessment to control for LPS exposure (Supplemental Fig. S1B). Although the overall group does not show significance, a large number of animals in the HIE group have significantly smaller brain volumes compared to the control and MIA group. There was a trend towards significance in a decrease of the whole brain volume that appears to be driven by the two-hit HIE animals ($F(2,18) = 3.270$, $p = 0.0615$, one-way ANOVA; **Figure 2A**). There were no significant differences in brain region volume when controlling for whole brain size (Supplemental Fig. S1C).

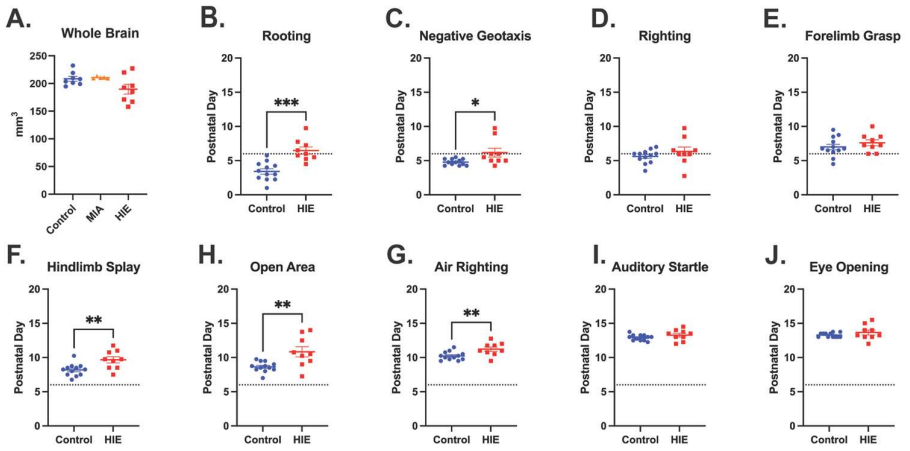

Figure 2. HIE results in a trend towards smaller brains 24 hours after injury, and motor developmental delays in the neonatal period. A) Whole brain volume obtained on P7 through ex vivo MRI for control animals, MIA only animals, and two-hit HIE animals. Analyzed with one-way ANOVA (n = 8 control; 5 MIA; 8 HIE). (B-J) Date of acquisition for neonatal developmental behaviors is shown for the average values for males and females in each litter. (n = 12 control; 9 HIE). The dashed line indicates hypoxia exposure (P6). Developmental behaviors were analyzed individually with a t-test unless they were not normally distributed, in which case they were analyzed via a Mann-Whitney test.

HIE animals had a significant delay in acquisition in five of the nine behavioral assessments including negative geotaxis, rooting, hindlimb splay, open area, and air righting. There was a significant main effect in delay of acquisition for HIE animals compared to control animals in the following behaviors: rooting ($t(19) = 4.777$, $p = 0.0001$, unpaired t-test; **Figure 2B**), negative geotaxis ($U = 24.50$, $p = 0.0343$, Mann-Whitney test; **Figure 2C**), hindlimb splay ($t(19) = 2.999$, $p = 0.0074$, unpaired t-test, **Figure 2F**), open area ($U = 16.50$, $p = 0.0057$, Mann-Whitney test, **Figure 2G**), and air righting ($t(19) = 2.896$, $p = 0.0193$, unpaired t-test; **Figure 2H**). There were no differences in righting

 doi:10.20944/preprints202407.2364.v1

($t(19) = 1.111$, $p = 0.2802$, unpaired t-test, **Figure 2H**), forelimb grasp ($t(19) = 1.008$, $p = 0.3259$, unpaired t-test; **Figure 2E**), auditory startle ($t(19) = 1.328$, $p = 0.1998$, unpaired t-test **Figure 2I**), or eye opening ($U = 42$, $p = 0.3972$ **Figure 2J**).

3.2. Non-Invasive Two Hit Model of HIE Results in Adult Motor Deficits in Gait and Grip Strength

In the catwalk assessment, stride length, swing, and speed were chosen a priori as parameters for analysis. HIE animals exhibited shorter stride length in both forepaws ($t(42) = 2.947$, $p = 0.0052$, unpaired t-test, **Figure 3A**) and hindpaws ($t(42) = 3.399$, $p = 0.0015$, unpaired t-test; **Figure 3A**). They also exhibited a shorter swing in hindpaws ($U = 133$, $p = 0.0110$, Mann-Whitney test ; **Figure 3B**), but not forepaws (U = 183, p = 0.1849, Mann-Whitney test; **Figure 3B**). Despite this difference in gait, they did not have any difference in overall body speed compared to controls ($t(42) = 0.5560$, $p = 0.5812$, unpaired t-test; **Figure 3C**). HIE animals had a weaker grip strength compared to controls ($F(1,74) = 9.867$, $p = 0.0024$, two-way ANOVA, **Figure 3D**), and females had a weaker grip strength compared to males ($F(1,17) = 18.89$, $p < 0.0001$). There was no interaction between HIE and sex ($F(1,74) = 0.095$, $p = 0.758$). Rotarod is a test of motor coordination and motor learning. HIE animals stayed on the rotarod significantly longer compared to controls ($p = 0.00376$, Coefficient = -0.4147, Hazard Ratio = 0.6605, 95% CI [0.499,0.8744], Cox mixed effects; **Figure 3E**). There were additionally no differences in either the three-chamber sociability test or the three-chamber social novelty test. (Supplemental Fig. S2B).

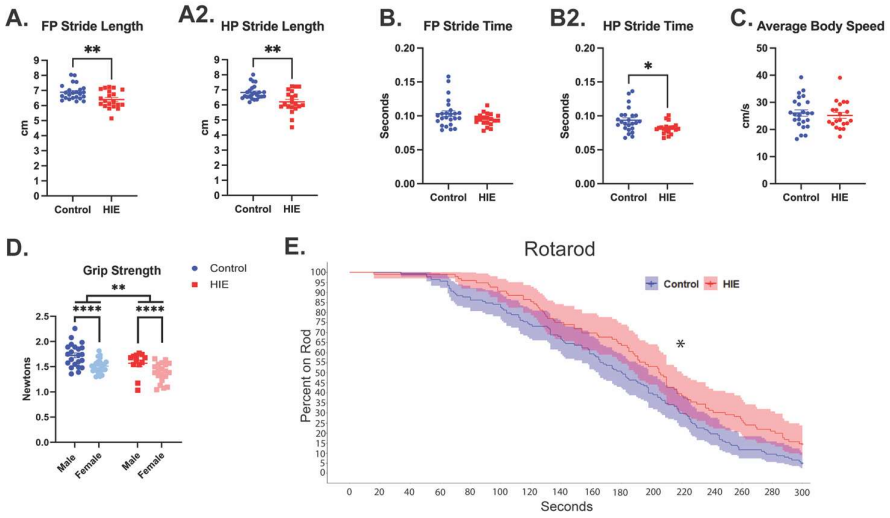

Figure 3. HIE results in distal muscle weakness and gait disturbances in adulthood. (A) forepaw (FP) and hindpaw (HP) stride lengths measured by the catwalk. **(B)** Forepaw and hindpaw swing time measured by the catwalk. **(C)** Average body speed on the catwalk. (catwalk n = 24 control; HIE = 20) **(D)** Forepaw strength measured by a grip strength meter (n = 22 control male, 24 control female; 12 HIE male, 20 HIE). **(E)** Survival curve showing the proportion of animals still on the rotating rod across time using a cox mixed effects model (n = 46 control; 32 HIE).

3.3. Non-Invasive Two Hit Model of HIE Produces Immediate Inflammatory Changes in Microglia

Microglia (CD11b+) cells were isolated from whole brains 24 hours following hypoxia. A total of 1335 genes were found to be differentially expressed with an FDR adjusted p-value of less than 0.05 by both edgeR and DESeq2. Of those, 157 were up-regulated and 1178 were down-regulated (**Figure 4**). A gene set enrichment analysis (GSEA) of mouse hallmark genes preranked by DEseq2 identified 15 significantly upregulated gene sets (FDR q-value < .05) (**Table 1**) and 4 downregulated gene sets (Supplemental Table S1). Several of the upregulated gene sets in microglia 24 hours following hypoxia represent a classical proinflammatory profile within microglia (TNFα via NFκB, Interferon -α and -γ responses, IL6/JAK/STAT3 Signaling, Inflammatory Response, Complement, IL2/STAT5

 doi:10.20944/preprints202407.2364.v1

Signaling, **Figure 4B**). Other gene sets represent the upregulation of cellular proliferation (MYC Targets V1, MYC Targets V2, PI3K/AKT/mTOR Signaling, and E2F targets, **Figure 4C**), as well as DNA damage checkpoint (G2M checkpoint), and apoptosis **(Figure 4D)**. A GSEA was performed on bulk RNAseq results from microglia isolated from whole brains collected 8 days following hypoxia. 215 genes were found to be differentially expressed with an FDR < .05 in both edgeR and DESeq2 (Supplemental Fig. S3). No gene sets were significantly different between groups at this time point.

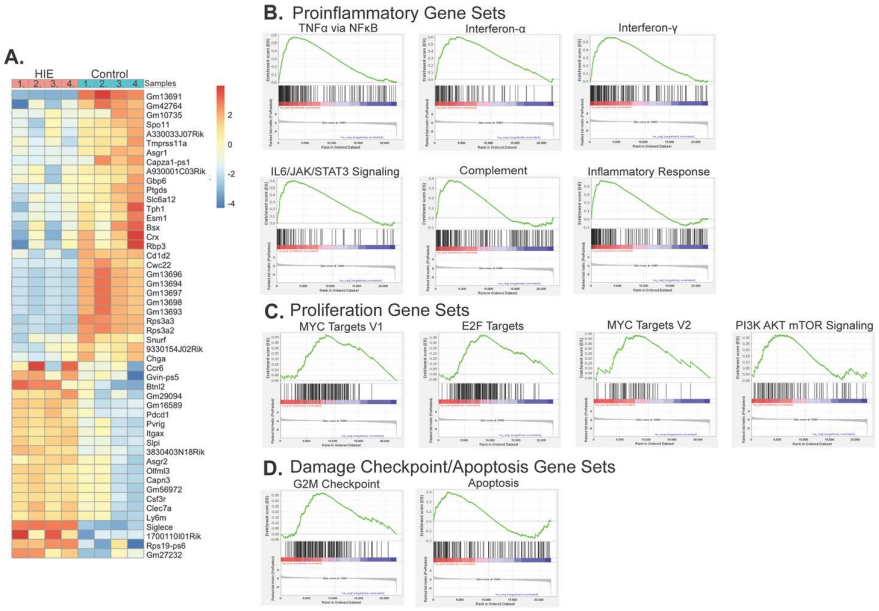

Figure 4. HIE results in acute transcriptional changes within microglia. (A) Genes identified by both DESeq2 and edgeR with an FDR adjusted p-value < .05 within CD11b+ cells one-day post hypoxia (n = 4 control, 4 HIE. **(B)** Gene set enrichment plots of significantly upregulated proinflammatory gene sets within HIE microglia. (C) Gene set enrichment plots of significantly proliferation-related gene sets within HIE microglia. (D) Gene set enrichment plots of significantly upregulated damage checkpoint/apoptosis gene sets within HIE microglia.

Table 1. Microglia Upregulated GSEA Analysis.

Hallmark Gene Set	ES	NES	FDR q-val	FWER p-val	Rank at Max
TNFα Signaling via NFκB	0.58	2.88	<0.001	<0.001	2773
Allograft Rejection	0.55	2.74	<0.001	<0.001	2202
Interferon-α Response	0.60	2.71	<0.001	<0.001	4120
Inferferon-γ Response	0.56	2.70	<0.001	<0.001	4099
IL6/JAK/STAT3 Signaling	0.60	2.66	<0.001	<0.001	3260
Inflammatory Response	0.47	2.39	<0.001	<0.001	1863
MYC Targets V1	0.42	2.06	<0.001	<0.001	8736
Complement	0.38	1.88	0.003	0.003	2945
E2F Targets	0.37	1.86	0.002	0.003	8678
G2M Checkpoint	0.37	1.84	0.004	0.005	8141
MYC Targets V2	0.44	1.81	0.004	0.005	8186
IL2 STAT5 Signaling	0.30	1.50	0.031	0.043	2156
PI3K AKT mTOR Signaling	0.32	1.50	0.029	0.043	5532
KRAS Signaling Up	0.30	1.45	0.035	0.057	1815
Apoptosis	0.30	1.43	0.037	0.065	2765

ES: Enrichment Score; NES: Normalized Enrichment Score; FDR: False Discovery Rate; FWR: Familywise-error Rate.

 doi:10.20944/preprints202407.2364.v1

3.4. Single Cell Sequencing Reveals Monocyte Subclusters of Interest in HIE

Thirteen microglia and 5 macrophage subclusters were identified (**Figure 5A & B**). No novel subclusters were observed in HIE vs. control animals in either cell type. Analysis for differentially expressed genes in microglia with significant HIE and subcluster interactions found 27 upregulated genes (**Table 2.1**) and 23 downregulated genes (**Table 2.2**). Genes with distinct subcluster locations were primarily in subclusters 7, 11, and 12, indicating that these may be subclusters of interest in the microglia response to HIE. GO Analysis of these subclusters' significantly over-expressed marker genes show that subcluster 7 (**Figure 5C**) and subcluster 12 (**Figure 5D**) are enriched for neuron and nervous system development pathways. Subcluster 11 only had two significant over-expressed marker genes, Hba-a1 and Hbb-bs, both of which are hemoglobin genes (Supplemental File S2).

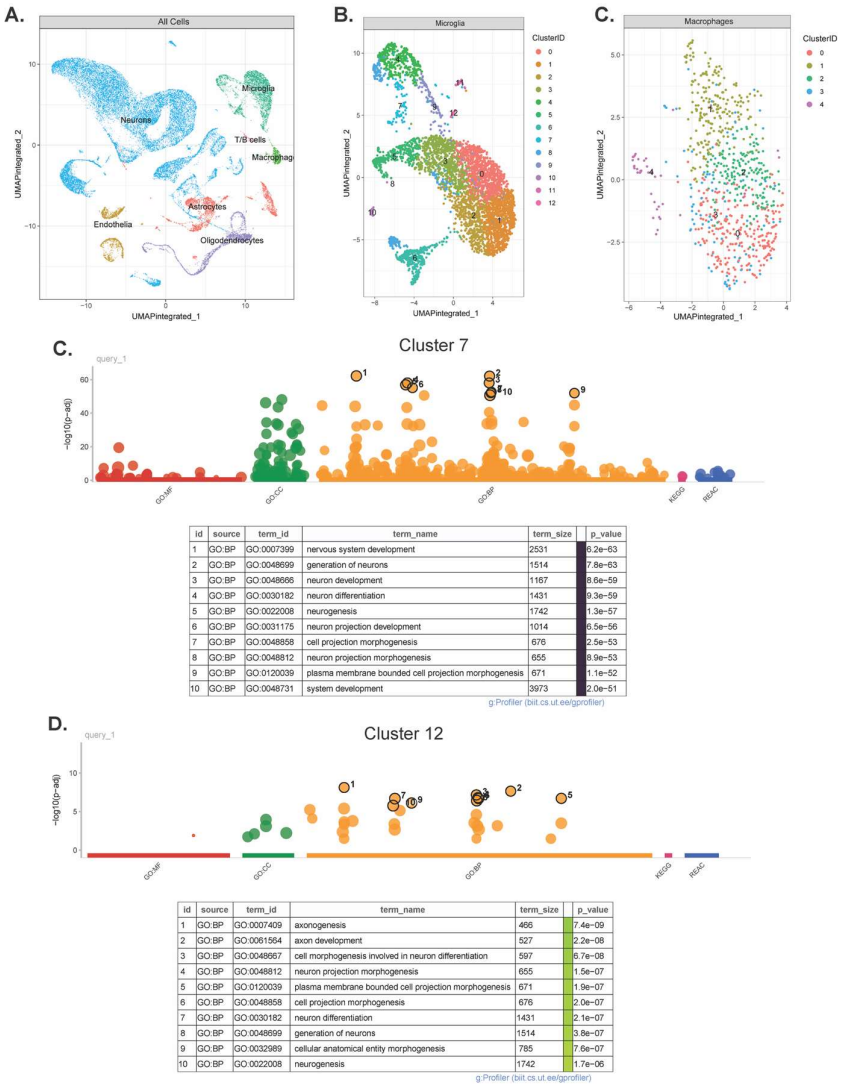

id	source	term_id	term_name	term_size	p_value
1	GO:BP	GO:0007399	nervous system development	2531	6.2e−63
2	GO:BP	GO:0048699	generation of neurons	1514	7.8e−63
3	GO:BP	GO:0048666	neuron development	1167	8.6e−59
4	GO:BP	GO:0030182	neuron differentiation	1431	9.3e−59
5	GO:BP	GO:0022008	neurogenesis	1742	1.3e−57
6	GO:BP	GO:0031175	neuron projection development	1014	6.5e−56
7	GO:BP	GO:0048858	cell projection morphogenesis	676	2.5e−53
8	GO:BP	GO:0048812	neuron projection morphogenesis	655	8.9e−53
9	GO:BP	GO:0120039	plasma membrane bounded cell projection morphogenesis	671	1.1e−52
10	GO:BP	GO:0048731	system development	3973	2.0e−51

id	source	term_id	term_name	term_size	p_value
1	GO:BP	GO:0007409	axonogenesis	466	7.4e−09
2	GO:BP	GO:0061564	axon development	527	2.2e−08
3	GO:BP	GO:0048667	cell morphogenesis involved in neuron differentiation	597	6.7e−08
4	GO:BP	GO:0048812	neuron projection morphogenesis	655	1.5e−07
5	GO:BP	GO:0120039	plasma membrane bounded cell projection morphogenesis	671	1.9e−07
6	GO:BP	GO:0048858	cell projection morphogenesis	676	2.0e−07
7	GO:BP	GO:0030182	neuron differentiation	1431	2.1e−07
8	GO:BP	GO:0048699	generation of neurons	1514	3.8e−07
9	GO:BP	GO:0032989	cellular anatomical entity morphogenesis	785	7.6e−07
10	GO:BP	GO:0022008	neurogenesis	1742	1.7e−06

Figure 5. (A) Representative UMAP of all cell types identified by scRNA-Seq**. (B)** Representative UMAP of identified microglia subclusters. **(C)** Representative UMAP of identified macrophage subclusters. **(D)** GO analysis of microglia subcluster 7. **(E)** GO analysis of microglia subcluster 12. (n = 12 control, 12 HIE).

Table 2.1. Upregulated Microglia genes with subcluster and HIE interaction.

Gene	baseMean	log2FC	lfcSE	stat	pvalue	padj
Astn2	30.49	2.952	1.64	44.22	1.40E-05	1.98E-03
Hba-a1	2142.28	2.279	1.73	70.31	2.80E-10	1.86E-07

 doi:10.20944/preprints202407.2364.v1

Hbb-bs	6555.16	1.885	1.62	72.37	1.15E-10	1.07E-07
Setbp1	35.02	0.817	0.57	49.92	1.44E-06	3.36E-04
Ptprd	37.61	0.770	0.55	41.20	4.53E-05	5.27E-03
Icam1	69.99	0.603	0.32	49.37	1.80E-06	4.00E-04
Tmtc2	16.38	0.509	1.18	40.00	7.18E-05	7.26E-03
Tuba1a	163.35	0.429	0.62	50.20	1.29E-06	3.15E-04
Hbb-bt	751.87	0.378	1.82	52.30	5.48E-07	1.59E-04
Nedd4l	45.40	0.362	0.31	44.38	1.32E-05	1.97E-03
Tubb2b	87.13	0.328	0.65	48.29	2.78E-06	5.57E-04
Nfia	199.82	0.317	0.28	55.88	1.26E-07	5.35E-05
Jun	891.49	0.188	0.29	40.09	6.94E-05	7.18E-03
Rgl1	43.30	0.186	0.21	39.80	7.76E-05	7.68E-03
Maml3	210.80	0.171	0.25	48.21	2.87E-06	5.57E-04
Jund	776.50	0.150	0.24	51.64	7.18E-07	1.86E-04
Dlc1	19.40	0.139	0.33	43.94	1.56E-05	2.08E-03
Ank2	64.41	0.134	0.33	47.34	4.08E-06	7.59E-04
Klf12	69.25	0.128	0.31	40.22	6.62E-05	7.00E-03
Tmsb10	118.80	0.105	0.37	44.61	1.20E-05	1.87E-03
Rtn1	110.34	0.093	0.46	87.06	1.83E-13	4.25E-10
Nav2	245.82	0.086	0.39	80.57	3.21E-12	4.98E-09
Chd7	72.15	0.078	0.20	45.32	9.10E-06	1.46E-03
Peli2	44.37	0.068	0.25	56.00	1.19E-07	5.35E-05
Ckb	219.35	0.065	0.17	55.52	1.46E-07	5.67E-05
Sumo2	138.34	0.048	0.14	41.08	4.75E-05	5.39E-03
Dock4	210.90	0.014	0.17	40.43	6.09E-05	6.59E-03

Table 2.2. Downregulated Microglia genes with subcluster and HIE interaction.

Gene	baseMean	log2FC	lfcSE	stat	pvalue	padj
Gramd1b	14.90	-1.315	0.49	44.12	1.45E-05	1.99E-03
Kif1b	38.76	-0.409	0.26	45.89	7.26E-06	1.30E-03
Mecp2	18.33	-0.348	0.31	45.57	8.23E-06	1.37E-03
Apc	65.68	-0.340	0.25	39.49	8.73E-05	8.13E-03
Ptprs	30.31	-0.269	0.36	54.00	2.73E-07	9.09E-05
Rfx7	21.30	-0.261	0.31	39.55	8.53E-05	8.10E-03
Nav3	414.56	-0.213	0.32	48.69	2.37E-06	5.01E-04
Tcf4	224.37	-0.200	0.25	74.41	4.76E-11	5.54E-08
Ttc3	63.26	-0.200	0.27	42.15	3.14E-05	3.75E-03
Ppp3ca	133.77	-0.199	0.15	44.22	1.40E-05	1.98E-03
Tnik	26.99	-0.149	0.94	45.56	8.27E-06	1.37E-03
Spag9	84.88	-0.131	0.20	54.55	2.18E-07	7.81E-05
Pld1	35.21	-0.121	0.20	40.65	5.60E-05	6.20E-03
Arsb	446.82	-0.104	0.12	39.69	8.10E-05	7.85E-03
Meis1	30.00	-0.097	0.54	55.87	1.26E-07	5.35E-05
Basp1	376.98	-0.094	0.14	129.34	8.39E-22	3.90E-18
Ssh2	174.40	-0.091	0.19	42.30	2.96E-05	3.63E-03
Ddah2	51.16	-0.066	0.28	42.97	2.29E-05	2.96E-03
Celf2	241.00	-0.064	0.39	71.32	1.82E-10	1.41E-07
Hsp90ab1	360.71	-0.060	0.10	68.87	5.20E-10	3.02E-07
Zbtb20	141.23	-0.057	0.28	53.38	3.52E-07	1.09E-04
Marcks	664.14	-0.052	0.09	42.31	2.95E-05	3.63E-03
Fosb	120.36	-0.033	0.31	52.02	6.16E-07	1.69E-04

 doi:10.20944/preprints202407.2364.v1

3.5. Single Cell Sequencing Reveals Changes in Microglia Motility, Macrophage Regulation of Neuron Development, and Epigenetic Pathway Upregulation in Macrophages after HIE

Pseudobulk RNAseq analysis of microglia and macrophages was performed using the single cell RNAseq data. In microglia, 125 genes were upregulated and 5 were downregulated (**Figure 6A**), and GO analysis revealed 218 significantly different pathways (**Figure 6C**). ReviGO analysis of the upregulated GO pathways demonstrates that microglia have significantly upregulated genes that are primarily involved in the actin cytoskeleton and cell motility (Supplemental Fig. S4). These include the biological processes of negative regulation of supramolecular fibers, actin polymerization, chemotaxis, cell localization, the molecular function of cytoskeletal protein binding, and the cellular components of anchoring junction, plasma membrane protein complex, lamellipodium, and actin cytoskeleton. There is also significant upregulation in genes involved in neuron development and synaptic signaling. In macrophages, 24 genes were upregulated and 6 genes were downregulated (**Figure 6B**), and GO analysis revealed 237 significantly different pathways (**Figure 6D**). ReviGO analysis of macrophages revealed biological processes primarily involved in neuronal and brain development (Supplemental Fig. S5). Changes in molecular function and cellular component genes point to upregulation of epigenetic changes specifically in the macrophage population (Supplemental Fig. S5). Interestingly, epigenetic changes were not seen in the microglia population.

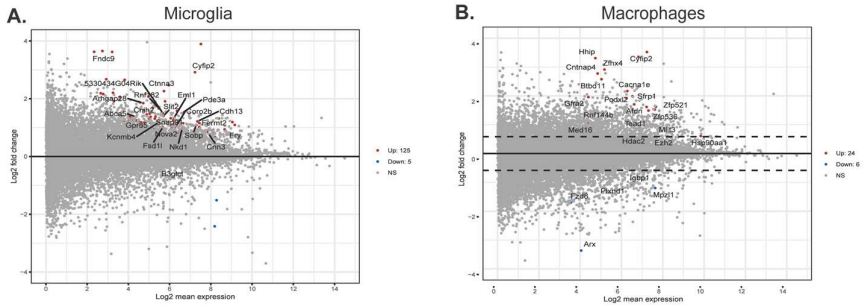

C. Microglia

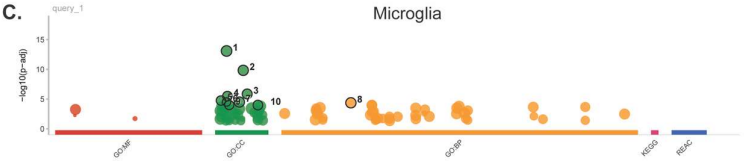

id	source	term_id	term_name	term_size	p_value
1	GO:CC	GO:0030054	cell junction	2230	8.3e−14
2	GO:CC	GO:0045202	synapse	1468	1.5e−10
3	GO:CC	GO:0070161	anchoring junction	905	1.4e−06
4	GO:CC	GO:0030424	axon	656	3.2e−06
5	GO:CC	GO:0005911	cell−cell junction	519	1.7e−05
6	GO:CC	GO:0030027	lamellipodium	202	3.0e−05
7	GO:CC	GO:0043005	neuron projection	1334	3.1e−05
8	GO:BP	GO:0016477	cell migration	1496	4.2e−05
9	GO:CC	GO:0031252	cell leading edge	427	9.9e−05
10	GO:CC	GO:0098794	postsynapse	650	1.0e−04

g:Profiler (biit.cs.ut.ee/gprofiler)

D. Macrophages

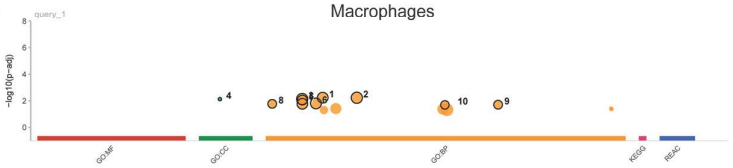

id	source	term_id	term_name	term_size	p_value
1	GO:BP	GO:0010604	positive regulation of macromolecule metabolic process	3420	5.8e−03
2	GO:BP	GO:0023052	signaling	6447	5.9e−03
3	GO:BP	GO:0007154	cell communication	6537	7.4e−03
4	GO:CC	GO:0035098	ESC/E(Z) complex	16	7.5e−03
5	GO:BP	GO:0007167	enzyme−linked receptor protein signaling pathway	967	8.8e−03
6	GO:BP	GO:0009893	positive regulation of metabolic process	3711	1.6e−02
7	GO:BP	GO:0007166	cell surface receptor signaling pathway	2799	1.7e−02
8	GO:BP	GO:0001822	kidney development	318	1.7e−02
9	GO:BP	GO:0072001	renal system development	328	2.0e−02
10	GO:BP	GO:0048863	stem cell differentiation	245	2.0e−02

g:Profiler (biit.cs.ut.ee/gprofiler)

Figure 6. Microglia and macrophages have significant transcriptional changes following HIE. (A) Volcano plot of the differentially expressed genes in microglia. **(B)** Volcano plot of the differentially

 doi:10.20944/preprints202407.2364.v1

expressed genes in macrophages. **(C)** Plot of the significantly different GO pathways in microglia by MF: molecular function, CC: cellular component, and BP: biological process. **(D)** Plot of the significantly different GO pathways in macrophages. (n = 12 control, 12 HIE).

4. Discussion

This novel two-hit mouse model of neonatal HIE uniquely allows for the investigation of maternal risk factors in the pathogenesis of HIE. Specifically, maternal infection and inflammation are optimally investigated in this system. This model also poses advantages over the traditional Rice-Vannucci model because it is non-invasive and does not require exposure to anesthesia, which raises concern for added neurotoxicity **[35]**. Our model utilizes maternal immune activation on GD18, considered equivalent to the third trimester of pregnancy in humans **[36]**, and a short severe global hypoxia on P6, considered equivalent to late preterm in human infants **[37]**. The two-hit model of neurodevelopmental disorders suggests that early life adversity such as MIA leads to increased risk in combination with a later stressorhttps://www.zotero.org/google-docs/?akRJ6j **[38]**. MIA has been shown to lead to alterations in immune response following a second immune challenge or stressor **[14,38]**, and prior studies demonstrated that MIA leads to exacerbated immune and autism-like behavioral outcomes when followed by the Rice-Vannucci model of HIE **[39]**. This is thought to occur through microglia priming which occurs when microglia become sensitized after entering a proinflammatory state following an initial stressor. However, the two-hit hypothesis of MIA has not been observed in all cases of non-immune second hits **[40]**.

Ex vivo MRI resulted in a trend towards significance with two-hit HIE animals exhibiting a relative decrease in whole brain volume only one day following the second hit of hypoxia. The lack of significance may be due to a higher variability in HIE animals as outcomes following HIE injury are often heterogeneous. Maternal immune activation (MIA) only animals were included in only this measure to control for the effects of LPS on overall pup size. However, the MIA animals had similar brain volumes to controls. These results are similar to those in humans, where infants have demonstrated decreased subcortical brain volumes acutely following injury **[41]**.

HIE animals exhibited delays in acquisition of developmental reflexes and behaviors predominantly in motor domains, supporting a phenotype comparable to that in human infants after HIE **[42,43]**. Some of the delays were in skills acquired by controls prior to the second hit of hypoxia on P6, indicating that maternal immune activation alone is responsible for at least some degree of developmental delay. However, the brain MRI volumetric differences indicate that LPS alone is not sufficient to decrease overall brain size, supporting the idea that the two hits are necessary for the full phenotype. This study aimed to describe the full two-hit model of HIE and did not parse the two-hits individually. Future studies can further elucidate the individual and combined effects of MIA and hypoxia within this model.

In the catwalk gait analysis, HIE animals had shorter overall stride lengths, and shorter hind paw stride times, indicating that they took shorter and quicker steps when compared with controls. Similar gait disruptions have been observed in other models of HIE **[18]**. Despite the changes in grip strength and gait, HIE animals performed better on the rotarod. As the rotarod test involves the animals staying on a small rod accelerating in rotation, the specific perturbations in gait observed in these animals may be beneficial to this test. Additionally, the test was censored at 300 seconds when the rod was no longer accelerating. A longer test or a test at a set speed may assess endurance more directly, which may be impacted in these animals. Despite the rotarod results, the changes in gait and the forelimb weakness observed in grip strength support motor dysfunction in adulthood in HIE animals. In the three-chamber behavioral task, the controls exhibited a high variability in discrimination ratio in both the sociability and social novelty. This indicates an issue with how the animals are performing this task at baseline and makes it difficult to assess any changes due to HIE exposure.

A limitation of our model is the lack of significant interactions between sex and HIE in any of the outcomes. This lack of sex differences is surprising given that MIA and other HIE models often show worse outcomes in males **[14,18,44]**. In humans, males have traditionally been thought to have

 doi:10.20944/preprints202407.2364.v1

higher rates of both morbidity and mortality, as well as higher occurrences of developmental delay and disorders following HIE **[45]**. However, clinical trials do not often report scores for males separately **[44]**. Some more recent clinical trials have shown little differences in males and females in control groups or following therapeutic hypothermia treatment **[46–48]**. This suggests that these sex differences may be less significant than originally thought and that treatment may additionally decrease these differences.

The two-hit model of HIE described here does not create the hemispheric, stroke-like focal injury common in the Rice-Vannucci model. While this was the intended goal of this model, it is more difficult to confirm injury presence, severity, and location. The focus of this study was to confirm the motor phenotype within this model throughout the lifespan as well as the acute inflammatory profile following injury. Our findings of long-lasting motor deficits and proinflammation within microglia suggest that neural changes are taking place within our model. This is supported by the relative decrease in overall brain volume at 24 hours following hypoxia. Future studies of this model will utilize histological methods to determine the extent and location of injury, as well as investigate white matter disruptions that are typical in HIE injury.

Neuroinflammation is immediately apparent in our model of HIE and can be seen within the first 24 hours with an upregulation of multiple proinflammatory pathways including TNF-α signaling via the NF-κB pathway. The upregulation of G2M checkpoint and apoptosis pathways indicate cellular damage and death, while the upregulation of proliferation markers MYC targets (V1 and V2), PI3K/AKT/mTOR signaling, and E2F targets **[49–52]** suggest that the undamaged cells have increased proliferation as a mechanism of the proinflammatory response. While some upregulated gene sets are not specifically relevant to microglia (Allograft rejection, Kras Signaling Up) they likely represent an upregulation in proinflammatory and proliferation genes respectively. This increase in proliferation, inflammation, and cell death occurs only in the acute (24-hour) microglia response and returns to baseline one week later (P14). This is an important validation of our model as inflammation following hypoxic ischemic events is a well-established method of secondary injury, and often the target of therapeutics within preclinical models **[53]**.

Single cell RNA sequencing revealed 13 microglia cell clusters and 5 macrophage cell clusters within the mouse brain. There were no novel subpopulations that arose within the HIE group, however, differential gene expression within the clusters allowed us to identify 3 unique subpopulations; cluster 7, cluster 11, and cluster 12, that have a number of differentially expressed genes that are HIE-associated and cluster-associated. GO analysis of the top differentiating gene markers of these subclusters found that both cluster 7 and cluster 12 are largely involved in neurodevelopment, including axon and projection development. As this analysis was done at a later timepoint than the initial bulk RNAseq, the microglia may be primarily involved in neuronal repair and promote resiliency following the initial increase in neuroinflammation.

Interestingly, pseudobulk RNAseq analysis identified upregulation of multiple genes involved in epigenetic regulation within the macrophage population, as well as neuron and brain development. Microglia are known to be highly involved in neurodevelopment **[54,55]**. However, when activated by an immune challenge or otherwise disrupted, microglia may not properly contribute to neuron developmental processes such as synaptic pruning, leading to neurodevelopmental disorders and deficits in cognition, motor function, and sensation **[56,57]**. The upregulation of these pathways in macrophages may indicate a compensatory mechanism that contributes to repair following injury and resiliency within the mouse brain. At this timepoint, both the macrophages and microglia may be in a repair state as indicated by the microglia subcluster analysis. Many of the pathways found to be upregulated in microglia pseudobulk analysis are involved in actin cytoskeleton structure and cell motility, indicating that these cells are highly mobile following HIE. Although there was no distinct upregulation in proinflammatory pathways at this timepoint, the microglia may be responding to chemokine release and moving to areas of injury.

Neonatal HIE leads to life-long impacts in affected infants. While therapeutic hypothermia has been effective in decreasing injury for some children, many children are left with variable degrees of lifelong disability, highlighting the critical need for additional therapies for neonatal HIE.

 doi:10.20944/preprints202407.2364.v1

Etiologically relevant models are critical to the development of effective therapies that can be successfully translated to humans. The two-hit model presented here replicates the largest perinatal risk factor for HIE and accurately maintains the maternal-fetal connection while presenting an easier and noninvasive method to induce injury in a murine model. This model also results in long-lasting motor deficits, acute brain volume changes, and a proinflammatory response within microglia, which are representative of the impacts of injury within humans.

Supplementary Materials: The following supporting information can be downloaded at the website of this paper posted on Preprints.org, File S1: Cell type gene markers, File S2: Microglia subcluster differentiating genes, Figure S1: Additional neonatal data Figure S2: Additional adult data, Figure S3: Microglia bulk RNAseq P14, Figure S4: Microglia ReviGO Analysis., Figure S5: Macrophage RE Microglia Downregulated GSEA Analysis P7, Table S1:

Author Contributions: Conceptualization, E.W., E.L., B.C., and J.S.; methodology, J.S., E.W., B.C., K.F., and E.L.; software, E.L., Q.Z. and K.S..; validation, E.L., B.C., A.E., Q.Z., K.S., S.D., and E.W.; formal analysis, E.L., B.C., A.E., S.A., T.L., Q.Z., S.D., K.F. E.W., and J.S.; investigation, E.L., B.C., A.E., S.A., Q.Z., V.L., and E.W.; resources, E.W., J.S., Q.Z., and K.F.; data curation, E.W., and Q.Z.; writing—original draft preparation, E.L.; writing—review and editing, E.L., B.C., A.E., S.A., T.L., Q.Z., S.D., K.F. E.W., and J.S. visualization, E.L., E.W., V.L., A.E., S.D., Q.Z., and K.F.; supervision, E.W.; project administration, E.W.; funding acquisition, E.W. All authors have read and agreed to the published version of the manuscript.

Funding: This work was supported by an Institutional Development Award (IDeA) from the National Institute of General Medical Sciences of the National Institutes of Health under grant number U54-GM104941 (PI: Hicks, Pilot PI: Wright-Jin) and NIH COBRE 3P20GM103653. 9/1/2022–8/31/2027. "Renewal of Delaware Center for Neuroscience Research". This work was also supported by funding from Nemours Children's Health Foundation.

Institutional Review Board Statement: The animal study protocol was approved by the Institutional Animal Care and Use Committee of Nemours Children's Health (protocol RSP21-27351-002 original approval 7/7/2021, most recent approval 7/3/2024) for studies involving animals.

Informed Consent Statement: Not applicable.

Data Availability Statement: Bulk RNAseq data and single cell RNAseq data will be available in the GEO database. All other data is available upon request.

Acknowledgments: We thank Jordan Case for her help in determining the timing of our model, and Dr. Sayera Muqarram for her help in behavioral scoring. We thank David Harary for his useful comments and the Nemours Neuroscience community for their support and constructive feedback in developing this manuscript. We thank Dr. Amanda Hernan and Dr. Matt Butchbach for the use of their behavioral spaces and apparatuses. Figure 1A was created with BioRender.com.

Conflicts of Interest: The authors declare no conflicts of interest.

References

1. Kurinczuk, J.J.; White-Koning, M.; Badawi, N. Epidemiology of neonatal encephalopathy and hypoxic-ischaemic encephalopathy. *Early Hum Dev* **2010**, *86*, 329-338, doi:10.1016/j.earlhumdev.2010.05.010.
2. Namusoke, H.; Nannyonga, M.M.; Ssebunya, R.; Nakibuuka, V.K.; Mworozi, E. Incidence and short term outcomes of neonates with hypoxic ischemic encephalopathy in a Peri Urban teaching hospital, Uganda: a prospective cohort study. *Matern Health Neonatol Perinatol* **2018**, *4*, 6, doi:10.1186/s40748-018-0074-4.
3. Evans, K.; Rigby, A.S.; Hamilton, P.; Titchiner, N.; Hall, D.M. The relationships between neonatal encephalopathy and cerebral palsy: a cohort study. *J Obstet Gynaecol* **2001**, *21*, 114-120, doi:10.1080/01443610020025967.
4. Byrne, H.; Spencer, A.P.C.; Geary, G.; Jary, S.; Thoresen, M.; Cowan, F.M.; Brooks, J.C.W.; Chakkarapani, E. Development of the corpus callosum and cognition after neonatal encephalopathy. *Ann Clin Transl Neurol* **2023**, *10*, 32-47, doi:10.1002/acn3.51696.
5. Davidson, J.O.; Wassink, G.; van den Heuij, L.G.; Bennet, L.; Gunn, A.J. Therapeutic Hypothermia for Neonatal Hypoxic-Ischemic Encephalopathy - Where to from Here? *Front Neurol* **2015**, *6*, 198, doi:10.3389/fneur.2015.00198.
6. Natarajan, G.; Pappas, A.; Shankaran, S. Outcomes in childhood following therapeutic hypothermia for neonatal hypoxic-ischemic encephalopathy (HIE). *Semin Perinatol* **2016**, *40*, 549-555, doi:10.1053/j.semperi.2016.09.007.

7. Wassink, G.; Davidson, J.O.; Dhillon, S.K.; Zhou, K.; Bennet, L.; Thoresen, M.; Gunn, A.J. Therapeutic Hypothermia in Neonatal Hypoxic-Ischemic Encephalopathy. *Curr Neurol Neurosci Rep* **2019**, *19*, 2, doi:10.1007/s11910-019-0916-0.
8. Lundgren, C.; Brudin, L.; Wanby, A.S.; Blomberg, M. Ante- and intrapartum risk factors for neonatal hypoxic ischemic encephalopathy. *J Matern Fetal Neonatal Med* **2018**, *31*, 1595-1601, doi:10.1080/14767058.2017.1321628.
9. Landucci, E.; Pellegrini-Giampietro, D.E.; Facchinetti, F. Experimental Models for Testing the Efficacy of Pharmacological Treatments for Neonatal Hypoxic-Ischemic Encephalopathy. *Biomedicines* **2022**, *10*, doi:10.3390/biomedicines10050937.
10. Bao, M.; Hofsink, N.; Plosch, T. LPS versus Poly I:C model: comparison of long-term effects of bacterial and viral maternal immune activation on the offspring. *Am J Physiol Regul Integr Comp Physiol* **2022**, *322*, R99-R111, doi:10.1152/ajpregu.00087.2021.
11. Lu, Y.C.; Yeh, W.C.; Ohashi, P.S. LPS/TLR4 signal transduction pathway. *Cytokine* **2008**, *42*, 145-151, doi:10.1016/j.cyto.2008.01.006.
12. Smith, S.E.; Li, J.; Garbett, K.; Mirnics, K.; Patterson, P.H. Maternal immune activation alters fetal brain development through interleukin-6. *J Neurosci* **2007**, *27*, 10695-10702, doi:10.1523/JNEUROSCI.2178-07.2007.
13. Hall, M.B.; Willis, D.E.; Rodriguez, E.L.; Schwarz, J.M. Maternal immune activation as an epidemiological risk factor for neurodevelopmental disorders: Considerations of timing, severity, individual differences, and sex in human and rodent studies. *Front Neurosci* **2023**, *17*, 1135559, doi:10.3389/fnins.2023.1135559.
14. Chamera, K.; Szuster-Gluszczak, M.; Trojan, E.; Basta-Kaim, A. Maternal Immune Activation Sensitizes Male Offspring Rats to Lipopolysaccharide-Induced Microglial Deficits Involving the Dysfunction of CD200-CD200R and CX3CL1-CX3CR1 Systems. *Cells* **2020**, *9*, doi:10.3390/cells9071676.
15. Han, V.X.; Patel, S.; Jones, H.F.; Dale, R.C. Maternal immune activation and neuroinflammation in human neurodevelopmental disorders. *Nat Rev Neurol* **2021**, *17*, 564-579, doi:10.1038/s41582-021-00530-8.
16. Estes, M.L.; McAllister, A.K. Maternal immune activation: Implications for neuropsychiatric disorders. *Science* **2016**, *353*, 772-777, doi:10.1126/science.aag3194.
17. Raia-Barjat, T.; Digonnet, M.; Giraud, A.; Ayash, T.; Vancolen, S.; Benharouga, M.; Chauleur, C.; Alfaidy, N.; Sebire, G. Animal Models of Chorioamnionitis: Considerations for Translational Medicine. *Biomedicines* **2022**, *10*, doi:10.3390/biomedicines10040811.
18. Aravamuthan, B.R.; Gandham, S.; Young, A.B.; Rutkove, S.B. Sex may influence motor phenotype in a novel rodent model of cerebral palsy. *Neurobiol Dis* **2020**, *134*, 104711, doi:10.1016/j.nbd.2019.104711.
19. Hill, J.M.; Lim, M.A.; Stone, M.M. Developmental Milestones in the Newborn Mouse. In *Neuropeptide Techniques*, Gozes, I., Ed.; Humana Press: Totowa, NJ, 2008; pp. 131-149.
20. Home - Sentieon | Enable Precision Data for Precision Medicine. Available online: https://www.sentieon.com (accessed on 6/17/2024).
21. Dobin, A.; Davis, C.A.; Schlesinger, F.; Drenkow, J.; Zaleski, C.; Jha, S.; Batut, P.; Chaisson, M.; Gingeras, T.R. STAR: ultrafast universal RNA-seq aligner. *Bioinformatics* **2013**, *29*, 15-21, doi:10.1093/bioinformatics/bts635.
22. Li, B.; Dewey, C.N. RSEM: accurate transcript quantification from RNA-Seq data with or without a reference genome. *BMC Bioinformatics* **2011**, *12*, 323, doi:10.1186/1471-2105-12-323.
23. Robinson, M.D.; McCarthy, D.J.; Smyth, G.K. edgeR: a Bioconductor package for differential expression analysis of digital gene expression data. *Bioinformatics* **2010**, *26*, 139-140, doi:10.1093/bioinformatics/btp616.
24. Love, M.I.; Huber, W.; Anders, S. Moderated estimation of fold change and dispersion for RNA-seq data with DESeq2. *Genome Biol* **2014**, *15*, 550, doi:10.1186/s13059-014-0550-8.
25. Zheng, G.X.; Terry, J.M.; Belgrader, P.; Ryvkin, P.; Bent, Z.W.; Wilson, R.; Ziraldo, S.B.; Wheeler, T.D.; McDermott, G.P.; Zhu, J.; et al. Massively parallel digital transcriptional profiling of single cells. *Nat Commun* **2017**, *8*, 14049, doi:10.1038/ncomms14049.
26. Satija, R.; Farrell, J.A.; Gennert, D.; Schier, A.F.; Regev, A. Spatial reconstruction of single-cell gene expression data. *Nat Biotechnol* **2015**, *33*, 495-502, doi:10.1038/nbt.3192.
27. Subramanian, A.; Tamayo, P.; Mootha, V.K.; Mukherjee, S.; Ebert, B.L.; Gillette, M.A.; Paulovich, A.; Pomeroy, S.L.; Golub, T.R.; Lander, E.S.; et al. Gene set enrichment analysis: a knowledge-based approach for interpreting genome-wide expression profiles. *Proc Natl Acad Sci U S A* **2005**, *102*, 15545-15550, doi:10.1073/pnas.0506580102.
28. Liberzon, A.; Birger, C.; Thorvaldsdottir, H.; Ghandi, M.; Mesirov, J.P.; Tamayo, P. The Molecular Signatures Database (MSigDB) hallmark gene set collection. *Cell Syst* **2015**, *1*, 417-425, doi:10.1016/j.cels.2015.12.004.
29. Hao, Y.; Hao, S.; Andersen-Nissen, E.; Mauck, W.M., 3rd; Zheng, S.; Butler, A.; Lee, M.J.; Wilk, A.J.; Darby, C.; Zager, M.; et al. Integrated analysis of multimodal single-cell data. *Cell* **2021**, *184*, 3573-3587 e3529, doi:10.1016/j.cell.2021.04.048.

30. Hao, Y.; Stuart, T.; Kowalski, M.H.; Choudhary, S.; Hoffman, P.; Hartman, A.; Srivastava, A.; Molla, G.; Madad, S.; Fernandez-Granda, C.; et al. Dictionary learning for integrative, multimodal and scalable single-cell analysis. *Nat Biotechnol* **2024**, *42*, 293-304, doi:10.1038/s41587-023-01767-y.
31. Kolberg, L.; Raudvere, U.; Kuzmin, I.; Vilo, J.; Peterson, H. gprofiler2 -- an R package for gene list functional enrichment analysis and namespace conversion toolset g:Profiler. *F1000Res* **2020**, *9*, doi:10.12688/f1000research.24956.2.
32. PanglaoDB: a web server for exploration of mouse and human single-cell RNA sequencing data. Available online: https://academic.oup.com/database/article/doi/10.1093/database/baz046/5427041 (accessed on
33. Hu, C.; Li, T.; Xu, Y.; Zhang, X.; Li, F.; Bai, J.; Chen, J.; Jiang, W.; Yang, K.; Ou, Q.; et al. CellMarker 2.0: an updated database of manually curated cell markers in human/mouse and web tools based on scRNA-seq data. *Nucleic Acids Res* **2023**, *51*, D870-D876, doi:10.1093/nar/gkac947.
34. Pressler, R.; Auvin, S. Comparison of Brain Maturation among Species: An Example in Translational Research Suggesting the Possible Use of Bumetanide in Newborn. *Front Neurol* **2013**, *4*, 36, doi:10.3389/fneur.2013.00036.
35. Johnson, S.C.; Pan, A.; Li, L.; Sedensky, M.; Morgan, P. Neurotoxicity of anesthetics: Mechanisms and meaning from mouse intervention studies. *Neurotoxicol Teratol* **2019**, *71*, 22-31, doi:10.1016/j.ntt.2018.11.004.
36. Translating Time - Across Developing Mammalian Brains. Available online: https://www.translatingtime.org/ (accessed on 7/8/2024).
37. Semple, B.D.; Blomgren, K.; Gimlin, K.; Ferriero, D.M.; Noble-Haeusslein, L.J. Brain development in rodents and humans: Identifying benchmarks of maturation and vulnerability to injury across species. *Prog Neurobiol* **2013**, *106-107*, 1-16, doi:10.1016/j.pneurobio.2013.04.001.
38. Desbonnet, L.; Konkoth, A.; Laighneach, A.; McKernan, D.; Holleran, L.; McDonald, C.; Morris, D.W.; Donohoe, G.; Kelly, J. Dual hit mouse model to examine the long-term effects of maternal immune activation and post-weaning social isolation on schizophrenia endophenotypes. *Behav Brain Res* **2022**, *430*, 113930, doi:10.1016/j.bbr.2022.113930.
39. Chen, H.R.; Chen, C.W.; Mandhani, N.; Short-Miller, J.C.; Smucker, M.R.; Sun, Y.Y.; Kuan, C.Y. Monocytic Infiltrates Contribute to Autistic-like Behaviors in a Two-Hit Model of Neurodevelopmental Defects. *J Neurosci* **2020**, *40*, 9386-9400, doi:10.1523/JNEUROSCI.1171-20.2020.
40. Yee, N.; Ribic, A.; de Roo, C.C.; Fuchs, E. Differential effects of maternal immune activation and juvenile stress on anxiety-like behaviour and physiology in adult rats: no evidence for the "double-hit hypothesis". *Behav Brain Res* **2011**, *224*, 180-188, doi:10.1016/j.bbr.2011.05.040.
41. Kebaya, L.M.N.; Kapoor, B.; Mayorga, P.C.; Meyerink, P.; Foglton, K.; Altamimi, T.; Nichols, E.S.; de Ribaupierre, S.; Bhattacharya, S.; Tristao, L.; et al. Subcortical brain volumes in neonatal hypoxic-ischemic encephalopathy. *Pediatr Res* **2023**, *94*, 1797-1803, doi:10.1038/s41390-023-02695-y.
42. Sadeghi Moghaddam, P.; Aghaali, M.; Modarresy, S.Z.; Shahhamzei, S.; Aljaboori, M. Hypoxic Ischemic Encephalopathy Indicators of Sarnat and Sarnat Scoring in Neonatal Subjects with Perinatal Asphyxia. *Iran J Child Neurol* **2024**, *18*, 81-91, doi:10.22037/ijcn.v17i2.36967.
43. Alkan, H.; Kahraman, A.; Mutlu, A. Early Spontaneous Movements of Infants With Hypoxic-Ischemic Encephalopathy. *Pediatr Phys Ther* **2021**, *33*, 18-22, doi:10.1097/PEP.0000000000000759.
44. Smith, A.L.; Alexander, M.; Rosenkrantz, T.S.; Sadek, M.L.; Fitch, R.H. Sex differences in behavioral outcome following neonatal hypoxia ischemia: insights from a clinical meta-analysis and a rodent model of induced hypoxic ischemic brain injury. *Exp Neurol* **2014**, *254*, 54-67, doi:10.1016/j.expneurol.2014.01.003.
45. Kelly, L.A.; Branagan, A.; Semova, G.; Molloy, E.J. Sex differences in neonatal brain injury and inflammation. *Front Immunol* **2023**, *14*, 1243364, doi:10.3389/fimmu.2023.1243364.
46. Sewell, E.K.; Shankaran, S.; Natarajan, G.; Laptook, A.; Das, A.; McDonald, S.A.; Hamrick, S.; Baack, M.; Rysavy, M.; Higgins, R.D.; et al. Evaluation of heterogeneity in effect of therapeutic hypothermia by sex among infants with neonatal encephalopathy. *Pediatr Res* **2023**, *94*, 1380-1384, doi:10.1038/s41390-023-02586-2.
47. Wyatt, J.S.; Gluckman, P.D.; Liu, P.Y.; Azzopardi, D.; Ballard, R.; Edwards, A.D.; Ferriero, D.M.; Polin, R.A.; Robertson, C.M.; Thoresen, M.; et al. Determinants of outcomes after head cooling for neonatal encephalopathy. *Pediatrics* **2007**, *119*, 912-921, doi:10.1542/peds.2006-2839.
48. Jenkins, D.D.; Rollins, L.G.; Perkel, J.K.; Wagner, C.L.; Katikaneni, L.P.; Bass, W.T.; Kaufman, D.A.; Horgan, M.J.; Languani, S.; Givelichian, L.; et al. Serum cytokines in a clinical trial of hypothermia for neonatal hypoxic-ischemic encephalopathy. *J Cereb Blood Flow Metab* **2012**, *32*, 1888-1896, doi:10.1038/jcbfm.2012.83.
49. Stark, G.R., & Taylor, W. R. Analyzing the G2/M Checkpoint. In *Checkpoint Controls and Cancer: Volume 1: Reviews and Model Systems*, Schönthal, A.H., Ed.; Humana Press: 2004; pp. 51–82.
50. Grandori, C.; Eisenman, R.N. Myc target genes. *Trends Biochem Sci* **1997**, *22*, 177-181, doi:10.1016/s0968-0004(97)01025-6.
51. Yu, J.S.; Cui, W. Proliferation, survival and metabolism: the role of PI3K/AKT/mTOR signalling in pluripotency and cell fate determination. *Development* **2016**, *143*, 3050-3060, doi:10.1242/dev.137075.

52. Helin, K. Regulation of cell proliferation by the E2F transcription factors. *Curr Opin Genet Dev* **1998**, *8*, 28-35, doi:10.1016/s0959-437x(98)80058-0.
53. Zhou, K.Q.; Davidson, J.O. Targeting neuroinflammation after therapeutic hypothermia for perinatal hypoxic-ischemic brain injury. *Neural Regen Res* **2023**, *18*, 1261-1262, doi:10.4103/1673-5374.360174.
54. Cowan, M.; Petri, W.A., Jr. Microglia: Immune Regulators of Neurodevelopment. *Front Immunol* **2018**, *9*, 2576, doi:10.3389/fimmu.2018.02576.
55. Sominsky, L.; De Luca, S.; Spencer, S.J. Microglia: Key players in neurodevelopment and neuronal plasticity. *Int J Biochem Cell Biol* **2018**, *94*, 56-60, doi:10.1016/j.biocel.2017.11.012.
56. Matuleviciute, R.; Akinluyi, E.T.; Muntslag, T.A.O.; Dewing, J.M.; Long, K.R.; Vernon, A.C.; Tremblay, M.E.; Menassa, D.A. Microglial contribution to the pathology of neurodevelopmental disorders in humans. *Acta Neuropathol* **2023**, *146*, 663-683, doi:10.1007/s00401-023-02629-2.
57. Arcuri, C.; Mecca, C.; Bianchi, R.; Giambanco, I.; Donato, R. The Pathophysiological Role of Microglia in Dynamic Surveillance, Phagocytosis and Structural Remodeling of the Developing CNS. *Front Mol Neurosci* **2017**, *10*, 191, doi:10.3389/fnmol.2017.00191.